

Article

## Signal Enhancement and Tuning of Surface Plasmon Resonance in Au Nanoparticle/Polyelectrolyte Ultrathin Films

Guoqian Jiang, Akira Baba, Hiroshi Ikarashi, Risheng Xu, Jason Locklin, Khan Rana Kashif, Kazunari Shinbo, Keizo Kato, Futao Kaneko, and Rigoberto Advincula

*J. Phys. Chem. C*, **2007**, 111 (50), 18687-18694 • DOI: 10.1021/jp075986e

Downloaded from <http://pubs.acs.org> on December 16, 2008

### More About This Article

Additional resources and features associated with this article are available within the HTML version:

- Supporting Information
- Links to the 3 articles that cite this article, as of the time of this article download
- Access to high resolution figures
- Links to articles and content related to this article
- Copyright permission to reproduce figures and/or text from this article

[View the Full Text HTML](#)



ACS Publications  
High quality. High impact.

# Signal Enhancement and Tuning of Surface Plasmon Resonance in Au Nanoparticle/Polyelectrolyte Ultrathin Films

Guoqian Jiang,<sup>†</sup> Akira Baba,<sup>†,‡</sup> Hiroshi Ikarashi,<sup>§</sup> Risheng Xu,<sup>†</sup> Jason Locklin,<sup>†</sup> Khan Rana Kashif,<sup>†</sup> Kazunari Shinbo,<sup>‡,§</sup> Keizo Kato,<sup>‡,§</sup> Futao Kaneko,<sup>‡,§</sup> and Rigoberto Advincula<sup>\*,†</sup>

Department of Chemistry and Department of Chemical Engineering, University of Houston, Houston, Texas 77204-5003, Center for Transdisciplinary Research and Department of Electrical and Electronic Engineering, Niigata University, 8050 Ikarashi Ninocho, Nishi-ku, Niigata 950-2181, Japan

Received: July 28, 2007; In Final Form: September 25, 2007

Investigations on optical and dielectric properties of hybrid ultrathin layer-by-layer (LbL) films of gold nanoparticles (AuNPs) and polyelectrolytes under different pH conditions resulted in surface plasmon resonance (SPR) signal enhancement under attenuated total reflection (ATR) spectroscopy conditions. Theoretical considerations on the basis of the Maxwell–Garnett theory were made to compare with experimental results. LbL films with different layer architectures were fabricated from AuNPs and two polyelectrolytes: poly(allylamine hydrochloride) (PAH) and poly(styrene sulfonate) (PSS) on Au and Ag thin film substrates for ATR. UV–vis spectroscopy and SPR spectroscopy were applied to study LbL film growth and monitor SPR shift upon pH switching. The (PAH/AuNPs)<sub>x</sub> multilayers showed an interesting dual-responsive SPR change as a function of pH and distance between AuNP layers and metal film. The addition of (PAH/PSS)<sub>y</sub> layers was found to act as an effective cushion to enhance this SPR response due to the significant swelling/shrinking of the film. In the case of [(PAH/PSS)<sub>y</sub> + (PAH/AuNPs)<sub>x</sub>], both theoretical calculations and experimental results showed that the SPR response can either (a) move toward lower incident angle with a sharp peak shape upon swelling in pH = 2 or (b) shift to a higher angle with a broadened peak shape after contraction in pH = 10. This effect was found to be opposite to what is expected from LbL films made up of the polyelectrolytes alone. Moreover, increasing the distance between AuNPs and the metal films also decouples this enhancement effect. A two-wavelength experiment (red and green lasers) was used to quantitatively demonstrate this SPR response to pH switching. Finally, SPR imaging was employed to monitor the SPR change with pH switching between 2 and 10 on the [(PAH/PSS)<sub>4</sub> + (PAH/AuNPs)<sub>2</sub>] film. Thus, on the basis of the SPR spectroscopic and SPR imaging pH response, a reproducible and stable sensing system can be successfully fabricated with these films.

## Introduction

The optical properties of gold nanoparticles (AuNPs) are of great interest for nanoscale science and practical sensing applications.<sup>1</sup> The fabrication of three-dimensional arrays of AuNPs on flat substrates or thin films can be employed to tune and manipulate their optical properties. This also allows for characterization using surface sensitive spectroscopic and microscopic analytical methods. Because the excitation of surface plasmons (SP) at the surface can largely enhance the local optical field, they also have the potential for sensor applications.<sup>2</sup> Recently, Minko and co-workers have reported a nanosensor on the basis of the swelling–shrinking effect of polymer brushes, poly(2-vinylpyridine) (P2VP) with AuNPs.<sup>3</sup> Due to the thickness change of the polymer brushes induced by pH change, the surface plasmon absorption bands significantly shifted due to the aggregation properties of the AuNPs. More recently, Sugimoto and co-workers have also shown a film swelling property with AuNPs applied to an SPR biosensor chips.<sup>4</sup> They reported the fabrication of molecularly imprinted

polymer gels with embedded AuNPs, which caused signal enhancement due to the film swelling on the event of analyte binding.

The layer-by-layer (LbL) self-assembly is one of most convenient techniques to fabricate molecularly controlled multilayer films with multifunctional properties.<sup>5</sup> The adsorption process involves alternate deposition of cationic and anionic species such as polyelectrolytes and charged nanoparticles from solution. Recently, Rubner and co-workers reported a reversible molecular memory effect on the basis of pH-switchable swelling/shrinking transitions of LbL films assembled with a weak polyelectrolyte poly(allylamine hydrochloride) (PAH) and a strong polyelectrolyte poly(styrene sulfonate) (PSS), envisioning the possibility for drug delivery applications.<sup>6</sup> On the other hand, Kotov et al. investigated the dispersion behavior of AuNPs within LBL films affecting the surface plasmon absorption strongly by manipulating interparticle interactions.<sup>7</sup>

In the present study, LbL films with different architectures [(PAH/AuNP)<sub>x</sub>], [(PAH/PSS)<sub>x</sub> + (PAH/AuNPs)<sub>y</sub>], and [(PAH/AuNPs)<sub>x</sub> + (PAH/PSS)<sub>y</sub>] were fabricated from PAH, PSS, and AuNP aqueous solutions. Theoretical optical properties of UV–vis and SPR spectroscopy for these films were first considered. The spacing/interaction between AuNPs and the distance between the AuNPs and ATR substrates (Au and Ag films)

\* Author to whom correspondence should be addressed. E-mail: radvincula@uh.edu.

<sup>†</sup> University of Houston.

<sup>‡</sup> Center for Transdisciplinary Research, Niigata University.

<sup>§</sup> Department of Electrical and Electronic Engineering, Niigata University.

played an important role in tuning their optical and dielectric properties. Drude's free electron model and the Maxwell–Garnett model were used for the theoretical estimation of UV–vis and SPR curves for AuNPs dispersed in a polyelectrolyte cushion system. The experimental results from SPR spectroscopy were found to match indeed with the theoretical estimation. Furthermore, pH-switchable swelling/shrinking transition experiments were done to demonstrate tuning of their optical properties. Finally, SPR imaging was performed to detect the reflectivity change in response to pH on a micropatterned array format, giving further evidence of the enhanced optical properties of the hybrid AuNP/polyelectrolyte film.

## Experimental Section

**Materials.** All materials were used without further purification. Poly(allylamine hydrochloride) (PAH, MW = 70 000 g/mol), poly(sodium 4-styrenesulfonate), (PSS, MW = 70 000 g/mol), 3-mercaptopropylsulfonic acid (MPS), tetrabutylammonium borohydride (TBAB), decanoic acid (DA), 11-mercaptopropylundecanoic acid (MUA), and (3-aminopropyl)triethoxy silane (APS) were purchased from Aldrich. Didodecyltrimethylammonium bromide (DDAB) was supplied by Acros Organics. Gold chloride (AuCl<sub>3</sub>, 99.99%) was obtained from Alfa Aesar. MUA stabilized gold nanoparticles (6 nm) were synthesized following Peng's procedure.<sup>8</sup>

**Multilayer Preparation.** Deionized water used in all of the experiments and cleaning steps was purified by a Millipore filtration unit (Milli-Q Academic system, Millipore Corp) equipped with a 0.22 μm Millistack filter at the outlet. The resistivity was 18.0 MΩ·cm. Glass substrates (LaSFN9, *n* = 1.85 at λ = 633 nm) were cleaned by sonicating with 2% Hellmanex solution, Milli-Q water, and ethanol and stored in ethanol prior to use. The surface of the dried, clean glass substrates was functionalized by submerging into freshly distilled toluene along with 0.5 wt % APS at 95 °C for 2 h. To remove the physically adsorbed species, the solution was discarded and the substrates were sonicated in three successive steps by adding freshly distilled toluene, 1:1 acetone/toluene, and acetone for 15, 10, and 10 min, respectively. They were finally dried with pure N<sub>2</sub> and stored in 0.01 M HCl solution overnight (surface charging).

Thin gold and silver films with a thickness of 40–50 nm were prepared by thermal evaporation on LaSFN9 glass under high vacuum (10<sup>-7</sup> Torr). The films were then modified by immersing in a 1 mM MPS ethanol solution followed by rinsing with copious amounts of ethanol and dried with N<sub>2</sub> gas, affording a negatively charged surface. Solutions of 1 mg/mL PAH and PSS were used for deposition. AuNPs (~4.8 mg) were dissolved in 50 mL of Milli-Q water. Prior to the LBL deposition, the pH of AuNPs, PAH, and PSS aqueous solutions were adjusted to 10.5 ± 0.5, 9.5 ± 0.2, and 9.5 ± 0.2, respectively, with concentrated NaOH and HCl. It should be noted that the concentrations of the AuNPs and the polyelectrolytes solutions were slightly changed after this adjustment. The functionalized glass/Au/Ag slides were dipped in PAH and PSS solutions for 15 min and AuNPs solution for 20–30 min, with rinsing, drying, and measurements taken in between.

**UV–vis Spectrometry.** UV–vis solution and film spectra were recorded using an Agilent 8453 spectrometer to monitor the SPR peak of MUA capped AuNPs, multilayer growth (up to 7 bilayers) of PAH/AuNPs and surface plasmon absorbance peak shift upon pH switching.

**Atomic Force Microscopy (AFM) Profilometry.** After scratching carefully on the 9-bilayer PAH/AuNPs on gold

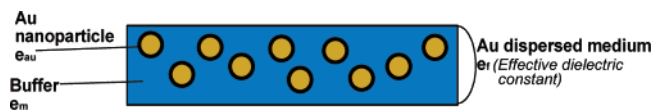


**Figure 1.** AuNPs dispersed medium used in MG calculation.

substrates, the thickness of the film was measured with Pt coated Si<sub>3</sub>N<sub>4</sub> cantilevers using contact mode (CM) AFM [PicoPlus System, Molecular Imaging (now Agilent Technologies), Tempe, AZ]. Results are shown in the Supporting Information.

**SPR Spectroscopy.** The spectra and deposition of LbL PAH/AuNPs films on a gold thin film were measured by angular-reflectivity scanning based on an attenuated total reflection (ATR) setup. This setup was used for the excitation of surface plasmons (noble metal films) or propagating surface plasmons in the classical Kretschmann configuration. The film thicknesses and dielectric constants were calculated by fitting the SPR curves with a Fresnel formula algorithm using the Winspall software (version 2.20, developed at the Max Planck Institute for Polymer Research, Mainz, Germany). SPR kinetics (with time) and full angle-reflectivity measurements were performed to study the LbL deposition of PAH/AuNPs and monitor pH induced swelling/shrinking of the films with different compositions.<sup>9</sup>

**SPR Imaging.** SPR imaging<sup>10</sup> was carried out to study the swelling/shrinking properties on a patterned surface. A setup used for the SPR imaging experiments has been previously reported.<sup>11</sup> A He–Ne laser (632.8 nm) passed through a special filter was irradiated on the patterned samples, and the reflected light was detected and imaged via CCD camera (Hamamatsu C5405). In this experiment, a micropatterned (PAH/PSS)<sub>4</sub>+ (PAH/AuNPs)<sub>2</sub> film on a Ag film substrate was used. The patterned Ag films (~45 nm thick) were prepared by evaporating Ag onto LaSFN9 glass slides covered by copper masks. The area not covered by the copper masks is where the Ag films deposited and the multilayer films were built up on these islands. The gridding size is about 400 microns. Prior to multilayer fabrication, the patterned films were dipped in a 1 mM MPS ethanol solution to modify the surface charge.

## Results and Discussions

**Theoretical Consideration: Optical Properties of Gold Nanoparticles Dispersed Medium (Surface Plasmon Absorption Band).** In order to estimate the optical properties of AuNPs in a dispersed medium, the effective dielectric function on the basis of the Maxwell–Garnett (MG) theory<sup>12</sup> and the effective medium approximation were used for simulation.<sup>13</sup> Figure 1 shows the modeled system, i.e., AuNPs dispersed medium.

The effective dielectric function derived from MG theory is given by<sup>14</sup>

$$\epsilon_f(\omega) = \epsilon'_f + \epsilon''_f = \epsilon_m + \frac{f(\epsilon'_{\text{au}} - \epsilon_m)\{\epsilon_m + \beta(\epsilon'_{\text{au}} - \epsilon_m) - f(\gamma\epsilon'_{\text{au}} - \epsilon_m)\} + f\epsilon''_{\text{au}}(\beta\epsilon''_{\text{au}} - f\gamma\epsilon''_{\text{au}})}{\{\epsilon_m + \beta(\epsilon'_{\text{au}} - \epsilon_m) - f(\gamma\epsilon'_{\text{au}} - \epsilon_m)\}^2 + (\beta\epsilon''_{\text{au}} - f\gamma\epsilon''_{\text{au}})^2} + i \left\{ \frac{f\epsilon''_{\text{au}}\{\epsilon_m + \beta(\epsilon'_{\text{au}} - \epsilon_m) - f(\gamma\epsilon'_{\text{au}} - \epsilon_m)\} - f(\epsilon'_{\text{au}} - \epsilon_m)(\beta\epsilon''_{\text{au}} - f\gamma\epsilon''_{\text{au}})}{\{\epsilon_m + \beta(\epsilon'_{\text{au}} - \epsilon_m) - f(\gamma\epsilon'_{\text{au}} - \epsilon_m)\}^2 + (\beta\epsilon''_{\text{au}} - f\gamma\epsilon''_{\text{au}})^2} \right\} \quad (1)$$

where  $\gamma$  is defined as

$$\gamma = \frac{1}{3\epsilon_m} + \frac{K}{4\pi\epsilon_m} \quad (2)$$

Parameter  $K$  represents the rate between the electric field generated by adjacent particles. When  $K = 0$ , it indicates that the dipole–dipole interaction between the particles is negligible.  $\beta$  is the parameter of the particle's shape. When the particle is a sphere,  $\beta$  becomes  $1/3$ . From this equation, the complex effective dielectric constant of the AuNPs dispersed medium can be calculated. The optical absorption spectrum of the AuNPs dispersed medium can also be derived from the effective dielectric function and is given by

$$\alpha = \frac{4\pi k(\omega)}{\lambda} = \frac{4\pi}{\lambda} \left( \frac{\sqrt{\epsilon'_f(\omega)^2 + \epsilon''_f(\omega)^2} + \epsilon'_f(\omega)}{2} \right)^{1/2} \quad (3)$$

where  $k(\omega)$  is extinction coefficient as a function of wavenumber.

The calculated absorption spectrum of AuNPs dispersed medium as a function of wavelength and filling factor,  $f$ , is shown in Figure 2. The absorption peak, i.e., surface plasmon band (localized surface plasmon), is clearly identifiable, shifting in absorbance and wavelength with variable filling factor. As previously reported, the surface plasmon band broadens and shifts toward higher wavelength with increase of the filling factor,<sup>9</sup> providing for a high contrast in SPR spectroscopy. This is deemed useful for sensor applications or monitoring AuNPs adsorption properties. Very recently, a similar simulation was done to estimate the AuNPs (diameter 20 nm)–DNA density on a flat Au surface.<sup>15</sup>

In this paper, we calculated the SPR curves (propagating SPR) as a function of filling factor of the AuNPs (localized SPR) in order to understand the AuNPs induced signal enhancement in the swelling–shrinking transition of the ultrathin films.

**Theoretical SPR Properties of AuNPs Adsorbed onto Flat Au Thin Film.** On the basis of the calculated effective dielectric function of AuNPs-dispersed medium using the MG model as shown above, the shift of SPR curves due to adsorption of AuNPs on a flat gold thin film was estimated by Fresnel calculation. The system used in this calculation is shown in Figure 3. This Kretschmann ATR geometry consists of prism/glass (LaSFN9), flat gold film (45 nm), gold nanoparticles (diameter 6 nm), and buffer (water). In this case, the effective dielectric constant of AuNPs dispersed layer is calculated from eq 1 as a function of filling factor and detailed further in the Supporting Information, Figure 1. The SPR curve calculation was carried out at the fixed wavelengths of 543 and 632.8 nm as a function of filling factor,  $f$ , ranging from 0.1 to 1.0 for comparison with experimental results (Figure 4). In the case of  $\lambda = 543$  nm (green laser), from  $f = 0.1$  to 0.5, the SPR curves shift toward higher incident angle (angle at the minimum) with increasing reflectivity at the minimum. When  $f$  is 0.5–0.7, the SPR curves still move to higher angles but the reflectivity at the minimum starts to decrease. Finally, the SPR curves shift to lower incident angle while the reflectivity at the minimum keeps decreasing. The saturation in terms of increase in the reflectivity at the minimum and its corresponding incident angle shift may be due to the high dielectric constant originating from the presence of the AuNPs and the propagating surface plasmon on the metal film/substrate. Since the effective dielectric constant shows a metal-like value when  $f$  is greater than 0.9 (very high density of AuNPs), the SPR resonance minimum appears at a lower angle than or comparable to the minimum of bare gold (Figure 4a). On the other hand, theoretical SPR curves at  $\lambda =$

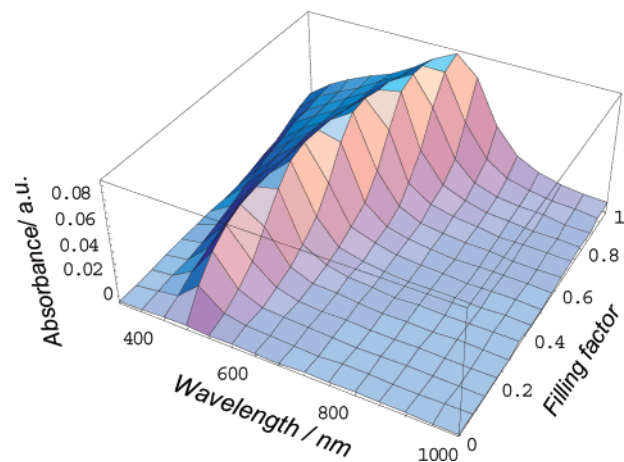


Figure 2. Calculated absorption spectrum of gold nanoparticles dispersed medium as functions of wavelength and filling factor. (a value of 6 nm was used for the diameter of nanoparticles).

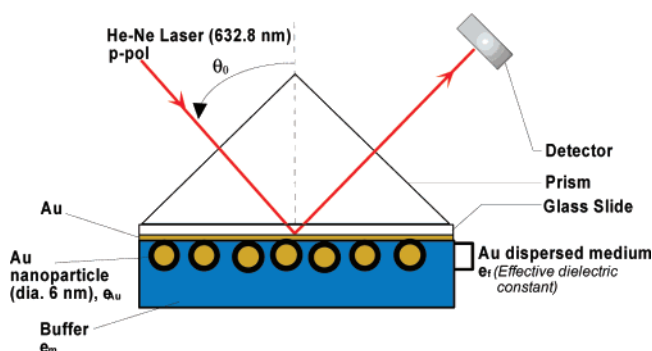
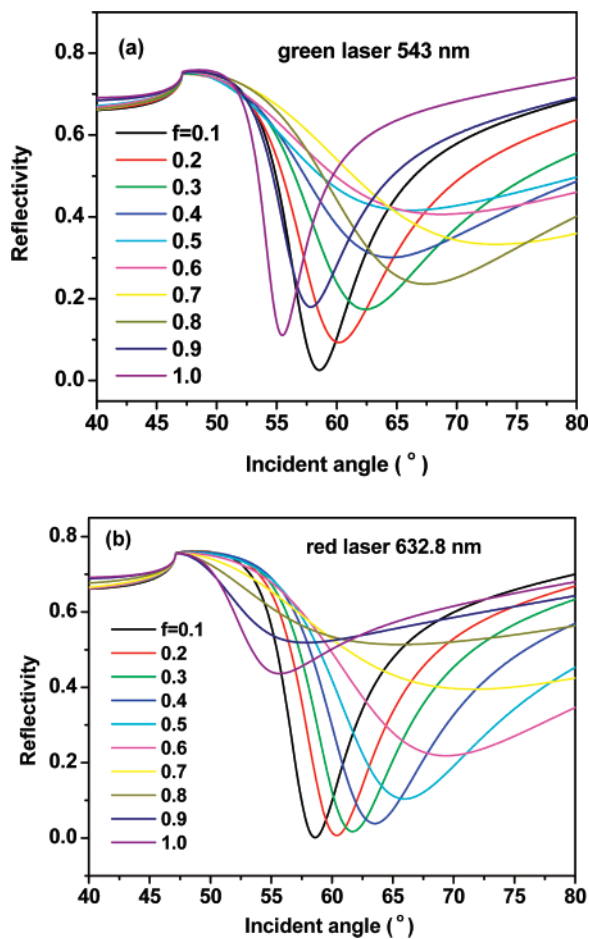


Figure 3. Prism/Au thin film/Au nanoparticle /buffer system used in the calculation.

632.8 nm (red laser) shifts toward higher angle with increase of the filling factor until  $f = 0.7$ . Then both the reflectivity at the minimum of the SPR curve and the SPR incident angle decrease from  $f = 0.8$  to 1.0 (Figure 4b). It is obvious from these calculations that the use of two wavelengths for excitation together with a densely packed AuNPs dispersion shows independent enhancement of the SPR signals, i.e., big changes in the resonance angle and minima, which should be very useful for sensor applications.

Figure 5 demonstrates the calculated SPR curves for the prism/Au flat thin film/ PAH–AuNPs/ water subphase system. The  $f$  values of the AuNPs in this configuration were assumed to be 0.1 and 0.2 before and after shrinking of the PAH film. As shown in this figure, the shrinking of the PAH film causes a densely packed AuNPs state in the multilayer system, so that the SPR curve shifts toward higher angles and broadens because the  $f$  of AuNPs increases with shrinking, while the SPR curve shifts to lower angle when the film swells. This calculation predicts that the sensitivity of the SPR curves is high even if the swelling–shrinking property is small. It should be noted that the direction of the minimum angle shift is opposite to the film swelling–shrinking property without the presence of AuNPs in the polyelectrolyte film.

**Fabrication of (PAH/AuNPs)<sub>x</sub>, (PAH/PSS)<sub>y</sub> + (PAH/AuNPs)<sub>x</sub>, and (PAH/AuNPs)<sub>x</sub> + (PAH/PSS)<sub>y</sub> LbL Ultrathin Films.** The deposition of PAH/PSS LbL films assembled at pH 9.5 solutions was studied<sup>6</sup> along with their thickness  $\sim 5$  nm for each bilayer. At first, UV–vis spectroscopy was used to monitor the PAH/AuNPs multilayer film growth. As seen from Figure 6, the PAH/AuNPs deposition resulted in a stepwise increase in the UV–vis absorbance, suggesting a linear growth



**Figure 4.** Calculated SPR curves of prism/Au thin film/gold nanoparticles/buffer system as a function of filling factor of gold nanoparticles under different light sources: (a) green laser,  $\lambda = 543$  nm; (b) red laser,  $\lambda = 632.8$  nm.

with respect to the film thickness when assembling the multilayers. The solution UV-vis spectrum of MUA-capped AuNPs (pH = 10–11) showed the surface plasmon peak to be centered at 515–530 nm (Figure 2 in the Supporting Information). On the other hand, the main absorption band in the thin solid film is  $\sim 25$ – $35$  nm red-shifted, which could be due to an increase of  $f$  (packing density), usually observed from AuNPs/polyelectrolyte films.<sup>16</sup> In addition, the center of the peak had a slight red shift with an increase in film thickness, indicating an enhancement of interparticle interactions due to the added dielectric layers<sup>17</sup> during the PAH/AuNPs LbL assembly.

SPR (ATR) spectroscopy was employed to study the film properties in terms of film thickness and dielectric constant. However, from the SPR angular curve, the film thickness cannot be readily determined because it depends on the assumption of a dielectric constant and vice versa. To determine the ultrathin film thickness and dielectric constant independently from SPR spectroscopy, two-color or multisubphase media methods are needed.<sup>18</sup> In the present study, independent thickness determination of the film was achieved using AFM profilometry. The 9-bilayer film was carefully scratched, and the thickness was determined using step-depth analysis. This thickness data was then used for the simulation of the corresponding SPR curve, giving the dielectric constant of the film. Finally, the calculated dielectric constant was applied to estimate the thicknesses of all other multilayered PAH/AuNPs films from 1 to 8 bilayers from the SPR angular curves. The film thickness for the 9-bilayer film by AFM profilometry was  $75 \pm 7$  nm, giving an

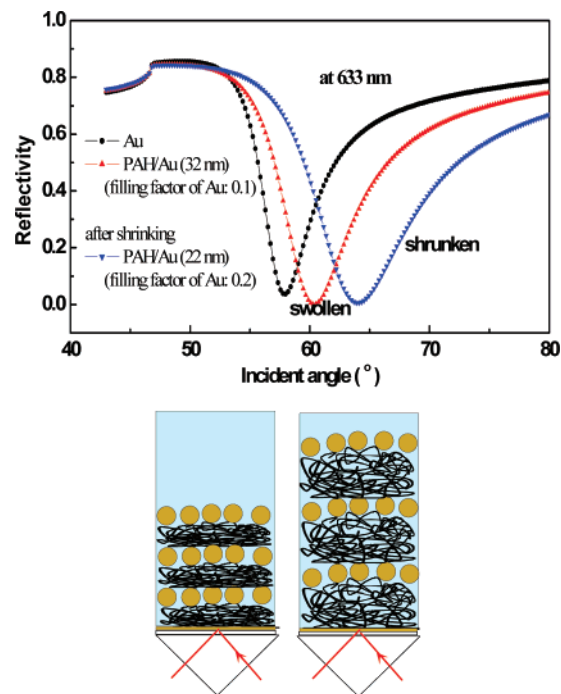


**Figure 5.** Calculated SPR curves of PAH/AuNPs before and after shrinking.

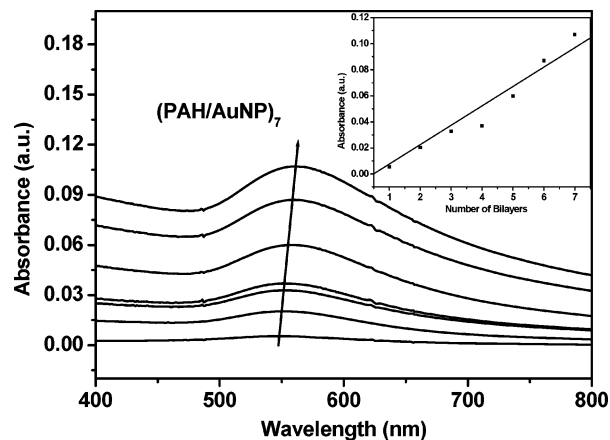


**Figure 6.** UV-vis spectrum of PAH/AuNPs LbL film on glass slide. The maximum absorption peak red-shifted from 550 nm on the first bilayer to around 560 nm on the seventh bilayer. The inset shows a linear increase of absorption intensity at the maximum peak with the increase of the film thickness.

average of  $8.3 \pm 0.8$  nm thickness for each bilayer using this method (Figure 3 in the Supporting Information). Therefore, in the simulation of the SPR curve, the thickness value of the 9-bilayer PAH/AuNPs film (75 nm) was fixed to estimate the average dielectric constant of the LbL film. On the basis of the Fresnel equation, the SPR angular curve for a 9-bilayer PAH/AuNPs film in water medium was simulated and the dielectric constant was determined to be 1.932. This dielectric constant value was then used for all of the other PAH/AuNPs films. As shown in Figure 7, the film thickness increases in a linear manner during the assembly. The average film thickness from the SPR angular scans was calculated to be  $\sim 8.0$  nm per bilayer, which is reasonable considering the dimension of PAH and the AuNPs size contribution.

**pH-Switchable Swelling/Shrinking Transition Experiments by UV-vis Spectroscopy: Surface Plasmon Resonance Spectroscopy and Imaging.** Recently, pH-responsive

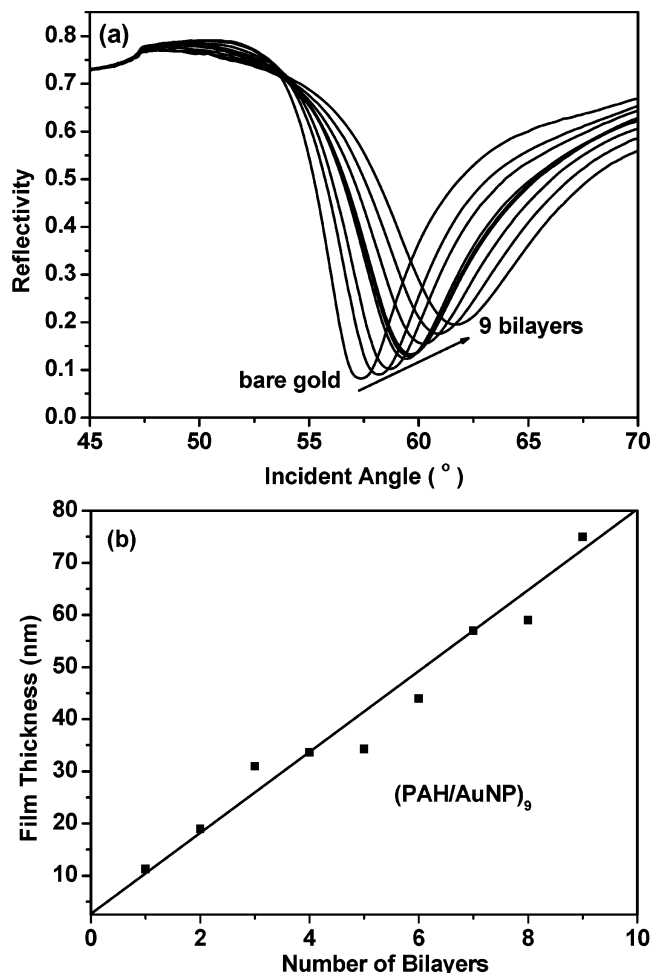


**Figure 7.** SPR angular curves of PAH/AuNPs 9-bilayer film (a), which gives an averaged 8.0 nm in thickness for each bilayer (b) by assuming the dielectric constant of the film to be 1.932, obtained from the SPR simulation of 9-bilayer film with 75 nm in thickness.

multilayered hybrid AuNPs/PAH microcapsules have been demonstrated.<sup>19</sup> The multilayered microcapsules assembled with carboxylic acid functionalized AuNPs and amino groups on PAH exhibits a dual pH-responsive property at both low and high pH. The swelling/shrinking transition experiments were initially attempted on a (AuNPs/PAH)<sub>10</sub> film assembled on BK7 glass slide for the detection of the SPR peak shift under pH 2 and 12 conditions. As observed from the UV-vis spectra in Figure 8, the film (AuNPs/PAH)<sub>10</sub> gives the SPR peak at ~545 nm in air. This wavelength is ~15 nm lower than the previous one as shown in Figure 6. This variation always exists, depending on many factors, such as size distribution of the initially prepared AuNPs and packing density of the AuNPs inside the film. When the contact medium was changed from pH 6 to 2, the center of the SPR peak moved from 545 to 537 nm. Upon changing the pH from 2 to 12, the peak further blue-shifted from 537 to 527 nm. Both blue shifts under low and high pH indicate a larger separation of the AuNPs distance, which is consistent with the previous study.<sup>19</sup> At pH = 2, the PAH layers were protonated and hence the charge density increased, leading to swelling of the polyelectrolyte layers. As a consequence, the alternated AuNPs layers were more separated. However, under pH 12, the PAH layers were deprotonated and the electrostatic interaction between the PAH films and the AuNPs layers was weakened. The weakening of the electrostatic interaction indirectly increased the charge density on the periphery of the AuNPs, leading to more repulsion among

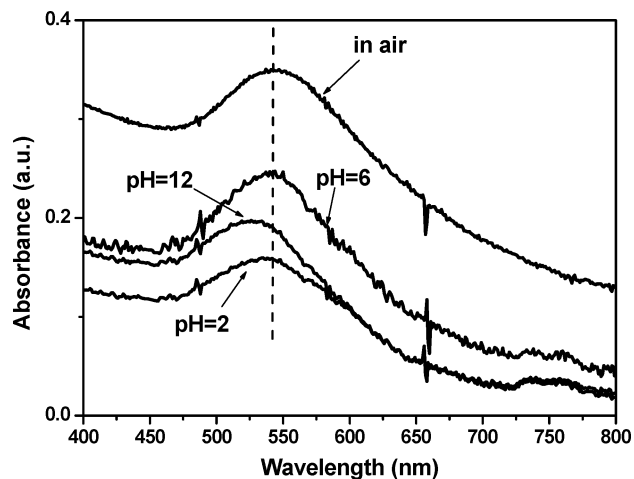


**Figure 8.** UV-vis spectra of the surface plasmon peaks of gold nanoparticles from the LbL film [(PAH/AuNPs)<sub>10</sub>] under different conditions (air, pH 6, 2, and 12).

nanoparticles. Thus, this resulted in weaker surface plasmon interactions among the AuNPs within each single layer.

SPR spectroscopy under ATR conditions is very sensitive to changes of the thin film properties in terms of thickness and dielectric constant. In the following SPR experiments, red and green lasers were used. Ag thin films on glass substrates were used due to the weak SPR of the gold film under green laser. Another modification was the introduction of PAH/PSS multilayer which acts as a cushion to PAH/AuNPs layers in the film. Compared to the [(AuNPs/PAH)<sub>10</sub>] films alone on a glass substrate in the UV-vis study, the [(PAH/PSS)<sub>5</sub> + (PAH/AuNPs)<sub>5</sub>] film on Ag substrate was fabricated for SPR swelling/shrinking transition experiments. With these modifications, well-defined SPR curves can be expected both under red and green lasers. Moreover, the distance from the AuNPs layers to the silver substrate can be tuned by adjusting the extent of shrinking/swelling of PAH/PSS cushion layers. The surface plasmon interactions between the AuNPs and the silver film can therefore be controlled. Therefore, both localized surface plasmon resonance from the nanoparticle and the propagating surface plasmon resonance from the ATR experiment can be accounted for. Figure 9a shows the SPR angular spectra for [(PAH/PSS)<sub>5</sub> + (PAH/AuNPs)<sub>5</sub>] LbL film in several switching pH cycles (pH = 6 → 2 → 12 → 2 → ...). The minimum angle of the reflectance plasmon curve shifted from ~70° to lower incidence angle (~60°) at pH = 2. Meanwhile, the curve shape turned to be very sharp and the SPR minima moved deeper. Then, the SPR curve shifted to higher angle (~62°) and broadened after changing the aqueous subphase to pH 12. By taking into account the theoretical estimations shown in Figures 4 and 5, the shift to higher angle and broadened curve indicates the existence of more densely packed AuNPs, i.e., shrinking effect of the films, whereas the shift to lower angle originates from a swelling effect. The other contribution is the stronger surface plasmon resonance coupling between AuNPs and the metal substrate, as reported by Tokareva et al.<sup>3</sup> This result agrees with other reports that PAH/PSS LbL films swell in lower pH (acidic) conditions and shrink in higher pH (basic) environment.<sup>6</sup> The AuNPs mutually enhanced the reflectivity SPR signals suggesting the possibility of a highly sensitive detection of swelling/shrinking switch, in which the nanoparticles can be independently functionalized while the overall response of the SPR signal in an ATR experiment can be monitored.

Moreover, the response properties of the AuNPs-enhanced SPR in terms of sensitivity and swelling/shrinking reversibility

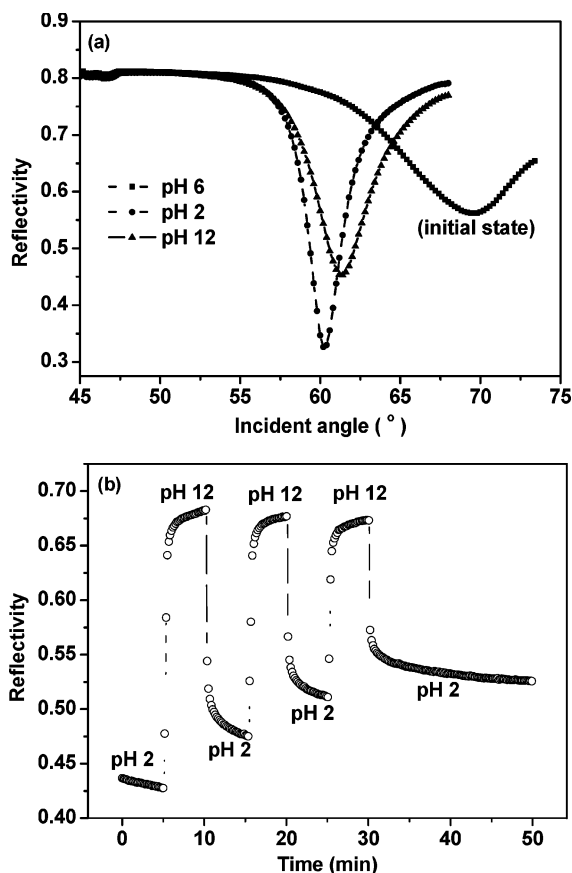


**Figure 9.** SPR measurements of [(PAH/PSS)<sub>5</sub> + (PAH/AuNPs)<sub>5</sub>]LbL film upon pH changing. (a) Angular measurements of the film in pH 6, 2, and 12. The angular curves were taken after the injection of pH 2 and 12; (b) kinetic curve of the film upon pH switch between 2 and 12. The switch was repeated three times.

are of crucial importance in the sensing applications. Figure 9b shows the SPR reflectivity change at fixed angle of 59° in three cycles between pH 2 and 12. The reflectivity increased rapidly upon shrinking during the first minute and then increased much more slowly with time. In a similar way, when the system was switched to pH 2, the reflectivity decreased drastically and then further decreased in a much slower manner. The fast response of this LbL film offers a rather simple and powerful sensing system. However, as we see from the amplitude, it gradually decreased with further cycling. It is not unreasonable if we consider that the degree of swelling/shrinking of the film is lower than the previous one as it goes toward an equilibrium state. However, this problem can be solved by simply elongating the first swelling/shrinking cycle time (Figure 4 in the Supporting Information). In order to investigate the time-dependent swelling/shrinking induced SPR properties, angular SPR curves were measured after 1, 60, 100, 120, 180, and 210 min in pH 12, as shown in Figure 10a. The SPR curves turned broader and shifted to higher angle with increasing time, indicating a continuous strengthening of SPR due to more closely packed AuNPs and shorter distance between the AuNPs and the silver substrate. This shrinking-induced SPR change was not found from the same LbL film assembled at pH 7.5 (data not shown), which indicates that the degree of ionization of weak polyelectrolytes in LbL films is insensitive to pH 2–12 switching unless the films are first assembled in a specific pH range.<sup>6</sup> Calculated SPR curves for different thickness of the PAH/PSS layers during the swelling/shrinking transition experiment were illustrated in Figure 10c. It is clear that with continuous shrinking of the film, the SPR curve shifts to higher incident angle and broadens

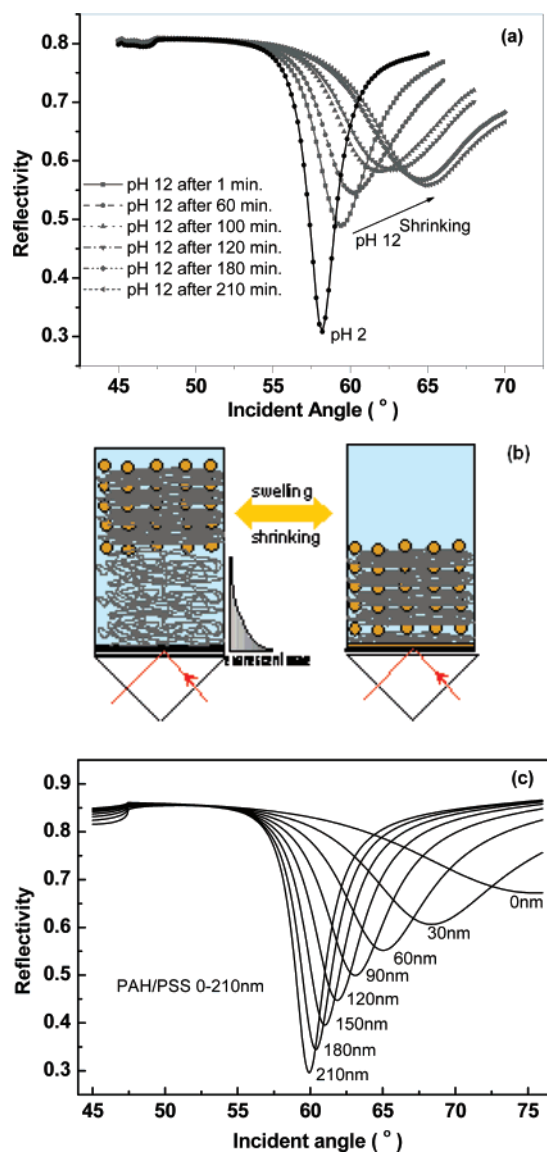


**Figure 10.** Time-dependent shrinking of [(PAH/PSS)<sub>5</sub> + (PAH/AuNPs)<sub>5</sub>]LbL film in pH 12. (a) SPR angular measurements under pH 2 and 12 at different measured time; (b) the swelling/shrinking transition scheme corresponding to the experiment in (a); (c) calculated SPR curves for different thickness of the PAH/PSS layers during the swelling/shrinking transition experiment in the prism/Ag/PAH-PSS/AuNPs/buffer system.

simultaneously. It is known that PAH/PSS film thickness can swell up to 5 times that of its original state as suggested from early studies.<sup>6b</sup> As seen from Figure 10c, as the PAH/PSS film swells from 30 to 150 nm, the SPR angle shifts from ~69° to ~61°. The 8° shift is highly comparable to the experimental data between pH 2 and 12 after 210 min in Figure 10a, indicating that the cushion layer PAH/PSS actually plays an important role in the tuning the SPR signal.

SPR two-color measurements were performed on the LbL films with different combinations: [(PAH/PSS)<sub>2</sub> + (PAH/AuNPs)<sub>2</sub>], [(PAH/PSS)<sub>2</sub> + (PAH/AuNPs)<sub>1</sub>], and [(PAH/AuNPs)<sub>2</sub> + (PAH/PSS)<sub>2</sub>]. In these control experiments, the distance between AuNPs and metal substrate plays an important role in the SPR angular change during swelling/shrinking. A recent study by He et al. on colloidal gold nanoparticles amplified SPR signals proposed that the distance (dielectric spacer) change between the AuNPs and noble metal substrates is more responsible for the SPR angle shifts than electromagnetic

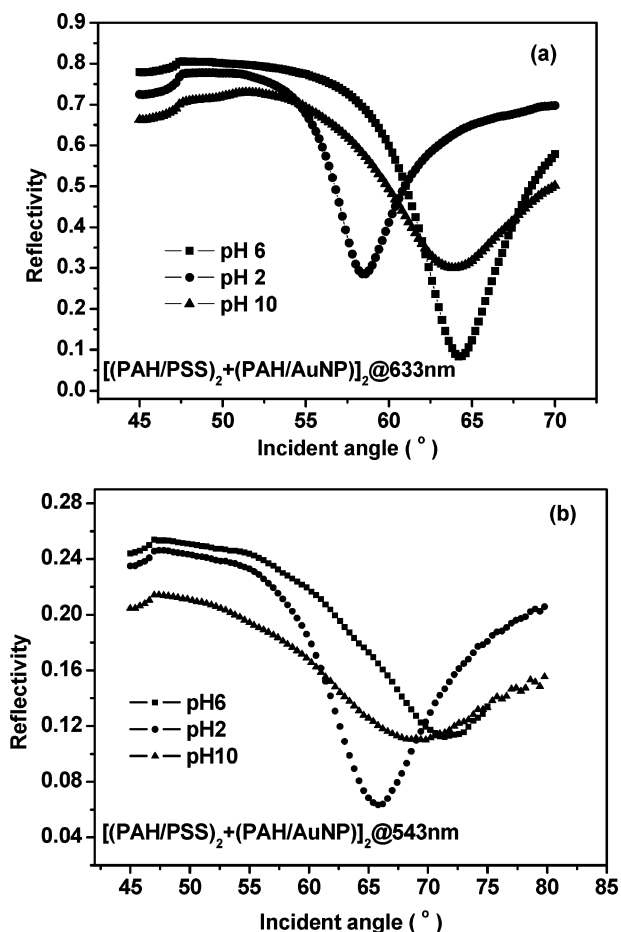


**Figure 11.** SPR two-color angular measurements on the LbL film  $[(\text{PAH/PSS})_2 + (\text{PAH/AuNPs})_2]$  under pH 6, 2, and 10. The injection order is pH 6 to 2 to 10. The light sources used here are red laser at 633 nm and green laser at 543 nm, respectively.

coupling.<sup>20</sup> As discussed previously, the SPR between the gold nanoparticles and the noble metal substrate increases after shrinking in basic condition ( $> \text{pH } 10$ ) and decreases after swelling under an acidic environment ( $< \text{pH } 3$ ). Figure 11 shows SPR angular measurements on the film  $[(\text{PAH/PSS})_2 + (\text{PAH/AuNPs})_2]$  by changing the pH from 6 to 2 to 10 under red laser at  $\lambda = 633 \text{ nm}$  and green laser at  $\lambda = 543 \text{ nm}$ . The result shown in Figure 11a is very similar to a previous experiment as shown in Figure 9a. One difference is that in Figure 11 the angular scanning was taken 2 h after each aqueous subphase (solution) injection considering the tendency toward an equilibrium state (maximum shrinking or swelling). The other difference is that the injected base solution is pH 10 instead of pH 12. Since pH 12 causes more shrinking of the film than pH 10, meaning higher angle shift, a larger separation between the pH 2 and 12 would be expected. Therefore, doing the angular scanning at a relatively long period of time after each pH water injection a larger separation between pH 2 and 10 angular curves can be expected (Figure 11). Thus, the SPR minima position and shape of the curves are dependent on the shrunken/swollen state of the film. The injection of the acidic and basic solution induces a continuous swelling and shrinking, affecting the AuNPs interaction.

As shown in Figure 11, the SPR curve was remarkably broader at the contracted state and became much sharper at the swollen state at 543 nm. This is because it is closer to the absorption peak of the initial state of AuNPs LbL film. Since the width of the SPR curve mostly depends on the imaginary part,  $\epsilon''$ , of dielectric constant or extinction coefficient, i.e.,

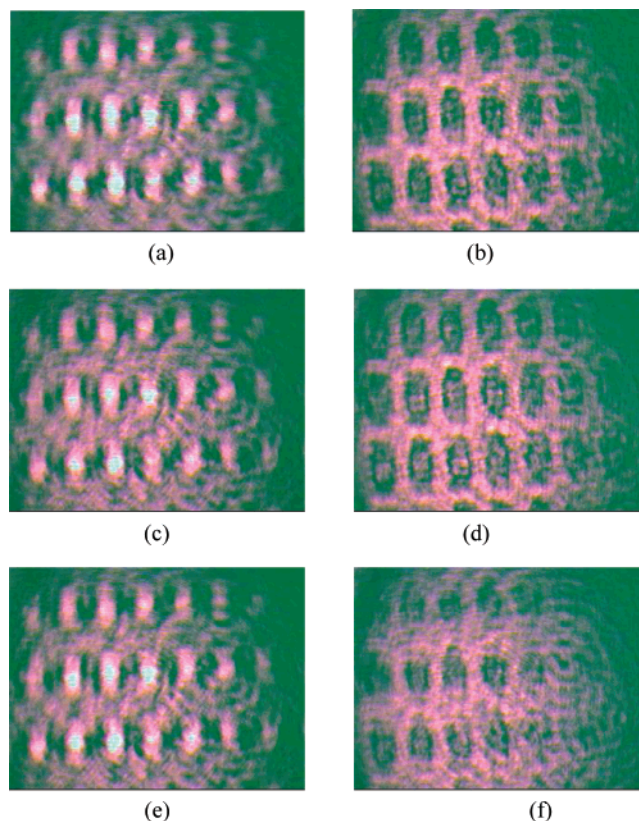


**Figure 12.** SPR imaging measurement on the film  $[(\text{PAH/PSS})_4 + (\text{PAH/AuNPs})_2]$  under different pH conditions. The images were assigned to (a) pH 6, (b) 2, (c) 10, (d) 2, (e) 10, and (f) 2 in a continuous order. Each image was taken 10 min after changing the different pH water except the first image was obtained immediately after pH 6 water was injected. All of the images were taken at a fixed angle of  $57.6^\circ$ . The lateral distance between each two pattern is about  $400 \mu\text{m}$ . The substrate is  $\sim 45 \text{ nm}$  Ag thin film.

absorption, this indicates that the absorption peak of the film is significantly changed between swollen and shrunken states.

In case of SPR angular measurements on the films  $[(\text{PAH/PSS})_2 + (\text{PAH/AuNPs})_1]$  (Figure 5a,b in the Supporting Information), i.e., less AuNPs layers, we can see similar results except that there is a smaller angle shift and less broadening after shrinking from the previously swollen state. However, when the film structure is  $[(\text{PAH/AuNPs})_2 + (\text{PAH/PSS})_2]$  (Figure 5c in the Supporting Information), i.e., the AuNPs are spaced from the Ag film with the cushion layers, no occurrence of this pH dependent SPR shift was found similar to the previous case. Instead, only the expected swelling/shrinking effects similar to a pure polyelectrolyte  $(\text{PAH/PSS})_2$  were observed. This is because the distance between the AuNPs and the silver film is increased ( $\sim 4\text{--}16 \text{ nm}$ ), decoupling the localized SPR of the AuNPs from the propagating SPR by the ATR experiment. This is another good proof that the distance between AuNPs and the substrate is a major factor for the SPR curve change. Thus, the SPR signal can also be easily tuned and enhanced by varying the  $(\text{PAH/PSS})$  cushion layers between the noble metal substrate and AuNPs containing layers.

**Surface Plasmon Resonance Imaging.** SPR imaging offers a direct visual observation of the SPR change for the AuNPs containing LbL films upon swelling/shrinking. Since the propagating SPR signal can be readily tuned by the electromagnetic coupling between AuNPs and the gold film, it can also be used for SPR imaging on patterned surfaces.<sup>2a, 21</sup> The LbL film with a composition  $[(\text{PAH/PSS})_4 + (\text{PAH/AuNPs})_2]$  was deposited on the patterned Ag substrate. In our SPR imaging

experiment, the incident angle was fixed at  $57.6^\circ$  and the CCD camera detected the intensity change of the reflected light under different pH conditions. As shown in Figure 12, after the injection of pH 2 solution, the bright area turned to dark, which is indicative of a shift to lower angle of the SPR curve. Then these dark patterns turned bright again upon pH 10 solution injection but still less bright than the image taken in pH 6, which supported the previous experimental results from the films [(PAH/PSS)<sub>5</sub> + (PAH/AuNPs)<sub>5</sub>] and [(PAH/PSS)<sub>2</sub> + (PAH/AuNPs)<sub>2</sub>]. The pH switching was repeated three times with very good reproducibility. It is possible to quantitatively analyze the brightness change from the CCD, although the intensity change can be readily and qualitatively correlated to the SPR angular curves measured on the films [(PAH/PSS)<sub>5</sub> + (PAH/AuNPs)<sub>5</sub>] and [(PAH/PSS)<sub>2</sub> + (PAH/AuNPs)<sub>2</sub>]. At the fixed angle of  $57.6^\circ$ , the reflectivity is the highest under pH 6. Upon pH 2 solution injection (swelling), the SPR minima moved to a lower angle than  $57.6^\circ$ . When a pH 10 solution was injected, the SPR curve shifted toward a higher angle. The reflectivity therefore changes within the vicinity of  $57.6^\circ$ , showing brighter patterns at higher pH, when the films contracts and lessening of brightness with swelling. However, they were still darker compared to the image at pH 6, which was at the most contracted state and has the highest SPR reflectance at this particular fixed angle (Figure 9a).

## Conclusions

Gold nanoparticles were used as a key component for SPR (ATR) signal enhancement in hybrid ultrathin films systems constructed using LbL deposition of a weak polyelectrolyte (PAH), a strong polyelectrolyte (PSS), and AuNPs. Theoretical calculations on the basis of MG theory were taken for elucidating the role of AuNPs in the SPR angular shift under different local environments as influenced by pH. Different LbL film architectures [(PAH/AuNPs)<sub>x</sub>], [(PAH/PSS)<sub>x</sub> + (PAH/AuNPs)<sub>y</sub>], and [(PAH/AuNPs)<sub>x</sub> + (PAH/PSS)<sub>y</sub>] were designed for UV-vis and SPR spectroscopy studies at different pH conditions. Two different wavelengths for excitation of the propagating plasmons (green and red) were used to better demonstrate the SPR signal enhancement. SPR imaging was finally applied as an alternative detection scheme for demonstrating the previous SPR properties of [(PAH/PSS)<sub>4</sub> + (PAH/AuNPs)<sub>2</sub>] films.

**Acknowledgment.** We thank Prof. Kaoru Tamada (Tokyo Institute of Technology) for helpful discussions. Funding from the Robert A. Welch Foundation (E-1551), NSF DMR-0504435, DMR-0602896, NSF-0330127, and the Alliance for NanoHealth of Texas is appreciated. A.B. acknowledges the NIH Keck Center Nanobiology Fellowship (NIH Grant No. 3 R90 DK071504-03).

**Supporting Information Available:** The calculations from green and red lasers to demonstrate the effective dielectric constants of gold nanoparticles (6 nm) as a function of the filling factor, UV-vis spectrum of the gold nanoparticles aqueous solution, AFM image and profilometry of the scratch on the

9-bilayer PAH/AuNPs film deposited on the gold substrate, SPR kinetic curves from pH 2 and 10 injections, and SPR angular measurements of the LbL films with two different combinations: [(PAH/PSS)<sub>2</sub> + (PAH/AuNPs)<sub>1</sub>] and [(PAH/AuNPs)<sub>2</sub> + (PAH/PSS)<sub>2</sub>]. This material is available free of charge via the web at <http://pubs.acs.org>.

## References and Notes

- (1) (a) Elghanian, R.; Storhoff, J. J.; Mucic, R. C.; Letsinger, R. L.; Mirkin, C. A. *Science* **1997**, *277*, 1078. (b) Link, S.; El-Sayed, M. A. *J. Phys. Chem. B* **1999**, *103*, 8410. (c) Daniel, M. C.; Astruc, D. *Chem. Rev.* **2004**, *104*, 293. (d) Barnes, W. L.; Dereux, A.; Ebbesen, T. W. *Nature* **2003**, *424*, 824. (e) Lyon, L. A.; Musick, M. D.; Smith, P. C.; Reiss, B. D.; Pena, D. J.; Natan, M. J. *Sens. Actuators B* **1999**, *54*, 118.
- (2) (a) He, L.; Musick, M. D.; Nicewarner, S. R.; Salinas, F. G.; Benkovic, S. J.; Natan, M. J.; Keating, C. D. *J. Am. Chem. Soc.* **2000**, *122*, 9071. (b) Cheng, S. F.; Chau, L. K. *Anal. Chem.* **2003**, *75*, 16. (c) Haes, A. J.; Zou, S. L.; Schatz, G. C.; Van Duyne, R. P. *J. Phys. Chem. B* **2004**, *108*, 109. (d) Haes, A. J.; Haynes, C. L.; McFarland, A. D.; Schatz, G. C.; Van Duyne, R. R.; Zou, S. L. *MRS Bull.* **2005**, *30*, 368.
- (3) Tokareva, I.; Minko, S.; Fendler, J. H.; Hutter, E. *J. Am. Chem. Soc.* **2004**, *126*, 15950.
- (4) Matsui, J.; Akamatsu, K.; Hara, N.; Miyoshi, D.; Nawafune, H.; Tamaki, K.; Sugimoto, N. *Anal. Chem.* **2005**, *77*, 4282.
- (5) (a) Decher, G.; Hong, J. D. *Makromol. Chem. Macromol. Symp.* **1991**, *46*, 321. (b) Decher, G. *Science* **1997**, *277*, 1232. (c) Advincula, R.; Fells, E.; Park, M.-K. *Chem. Mater.* **2001**, *13*, 2870. (d) Advincula, R.; Locklin, J.; Youk, J.; Xia, C.; Park, M.-K.; Fan, X. *Langmuir* **2001**, *18*, 877. (e) Park, M.-K.; Advincula, R. *Langmuir* **2002**, *18*, 4532. (f) Locklin, J.; Shinbo, K.; Onishi, K.; Kaneko, F.; Bao, Z.; Advincula, R. *Chem. Mater.* **2003**, *15*, 1404.
- (6) (a) Hiller, J.; Rubner, M. F. *Macromolecules* **2003**, *36*, 4078. (b) Itano, K.; Choi, J.; Rubner, M. F. *Macromolecules* **2005**, *38*, 3450.
- (7) Malikova, N.; Pastoriza-Santos, I.; Schierhorn, M.; Kotov, N. A.; Liz-Marzan, L. M. *Langmuir* **2002**, *18*, 3694.
- (8) Jana, N. R.; Peng, X. *J. Am. Chem. Soc.* **2003**, *125*, 14280.
- (9) (a) Knoll, W. *Annu. Rev. Phys. Chem.* **1998**, *49*, 569. (b) Baba, A.; Advincula, R. C.; Knoll, W. *J. Phys. Chem. B* **2002**, *106*, 1581. (c) Baba, A.; Park, M.-K.; Advincula, R. C.; Knoll, W. *Langmuir* **2002**, *18*, 4648.
- (10) Rothenhäusler, B.; Knoll, W. *Nature* **1988**, *332*, 615.
- (11) Baba, A.; Knoll, W. *Adv. Mater.* **2003**, *15*, 1015.
- (12) (a) Maxwell-Garnett, J. C. *Philos. Trans. R. Soc.* **1904**, *203*, 385. (b) Maxwell-Garnett, J. C. *Philos. Trans. R. Soc.* **1906**, *205*, 237.
- (13) Wu, Y. M.; Gao, L.; Li, Z. Y. *Phys. Status Solidi C* **2000**, *220*, 997.
- (14) (a) Ung, T.; Liz-Marzan, L. M.; Mulvaney, P. *J. Phys. Chem. B* **2001**, *105*, 3441. (b) Garcia, M. A.; Llopis, J.; Paje, S. E. *Chem. Phys. Lett.* **1999**, *315*, 313. (c) Ung, T.; Liz-Marzan, L. M.; Mulvaney, P. *Colloids Surf. A* **2002**, *202*, 119. (d) Link, S.; El-Sayed, M. A. *J. Phys. Chem. B* **1999**, *103*, 8410. (e) Li, X.; Tamada, K.; Baba, A.; Knoll, W.; Hara, M. *J. Phys. Chem. B* **2006**, *110*, 15755.
- (15) Ito, M.; Nakamura, F.; Baba, A.; Tamada, K.; Ushijima, H.; Lau, K. H. A.; Manna, A.; Knoll, W. *J. Phys. Chem. C* **2007**, *111*, 11653.
- (16) (a) Cho, J.; Caruso, F. *Chem. Mater.* **2005**, *17*, 4547. (b) Mayya, K. S.; Schoeler, B.; Caruso, F. *Adv. Funct. Mater.* **2003**, *13*, 183.
- (17) Jiang, C. Y.; Markutsya, S.; Tsukruk, V. V. *Langmuir* **2004**, *20*, 882.
- (18) (a) Peterlinz, K. A.; Georgiadis, R. *Langmuir* **1996**, *12*, 4731. (b) Georgiadis, R.; Peterlinz, K. P.; Peterson, A. W. *J. Am. Chem. Soc.* **2000**, *122*, 3166. (c) Tamada, K.; Akiyama, H.; Wei, T. X. *Langmuir* **2002**, *18*, 5239. (d) Jiang, G.; Baba, A.; Advincula, R. *Langmuir* **2007**, *23*, 817.
- (19) De Geest, B. G.; Skirtach, A. G.; De Beer, T. R. M.; Sukhorukov, G. B.; Bracke, L.; Baeyens, W. R. G.; Demeester, J.; De Smedt, S. C. *Micromol. Rapid Commun.* **2007**, *28*, 88.
- (20) He, L.; Smith, E. A.; Natan, M. J.; Keating, C. D. *J. Phys. Chem. B* **2004**, *108*, 10973.
- (21) Li, Y.; Wark, A. W.; Lee, H. J.; Corn, R. M. *Anal. Chem.* **2006**, *78*, 3158.